

LeFusion: Synthesizing Myocardial Pathology on Cardiac MRI via Lesion-Focus Diffusion Models

Hantao Zhang^{1*}, Jiancheng Yang^{2**}, Shouhong Wan¹, and Pascal Fua²

¹ University of Science and Technology of China (USTC), Hefei, China

² Swiss Federal Institute of Technology Lausanne (EPFL), Lausanne, Switzerland

Abstract. Data generated in clinical practice often exhibits biases, such as long-tail imbalance and algorithmic unfairness. This study aims to mitigate these challenges through data synthesis. Previous efforts in medical imaging synthesis have struggled with separating lesion information from background context, leading to difficulties in generating high-quality backgrounds and limited control over the synthetic output. Inspired by diffusion-based image inpainting, we propose LeFusion, lesion-focused diffusion models. By redesigning the diffusion learning objectives to concentrate on lesion areas, it simplifies the model learning process and enhance the controllability of the synthetic output, while preserving background by integrating forward-diffused background contexts into the reverse diffusion process. Furthermore, we generalize it to jointly handle multi-class lesions, and further introduce a generative model for lesion masks to increase synthesis diversity. Validated on the DE-MRI cardiac lesion segmentation dataset (Emidec), our methodology employs the popular nnUNet to demonstrate that the synthetic data make it possible to effectively enhance a state-of-the-art model. Code and model are available at <https://github.com/M3DV/LeFusion>.

Keywords: data synthesis · diffusion models · cardiac MRI · myocardial infarction · no-reflow phenomena.

1 Introduction

In most biomedical scenarios, the number of pathological subjects is significantly lower than that of normal ones. This discrepancy is primarily due to the naturally occurring distribution of patient data, which often exhibits a long-tail characteristic [32,34,25,29,30]. Furthermore, given potential biases in data collection, clinical data may be subject to algorithmic fairness [28,3], security, and privacy issues [19,20]. Thus, “synthetic data could be better than real data” [22].

Generative lesion synthesis is a promising area with applications across various medical modalities, achieving remarkable successes [12]. These include the synthesis of lung nodules [6,11,31] and COVID-19 lesions [16] in CT scans, colon polyp synthesis in colonoscopy [23,18,4], tumor cell synthesis in microscopy [8],

* This work was conducted during the first author’s research internship at EPFL.

** Corresponding author: Jiancheng Yang (jiancheng.yang@epfl.ch).

synthesized brain tumors in MRI [1], diabetic lesion synthesis in retinal images [26], synthetic skeleton breaks in pulmonary airways and vessels [27], and synthetic tumors in the liver [17]. Although many types of generative method have been explored, such as VAEs [13], GANs [5], and diffusion models [7], they often fail at producing high-quality backgrounds outside the lesion areas. While lesions might appear similar across different cases, which greatly helps when training human doctors, the background can vary significantly due to diverse imaging conditions. This is challenging for generative models, especially when they can only be trained using limited amounts of data.

Recent strategies we will refer to *controlled lesion synthesis* (CLS) [33,9] offer an alternative. These methods start from readily available normal scans and synthesize lesions into them. This involves generating lesion masks and the textures to fill them. This targeted approach ensures high-quality background generation and controllability. Its usefulness has been demonstrated to model COVID-19 lesions [33] and liver tumors [9]. However, these methods are heavily hand-crafted, with heuristics that is hard to generalize.

In this study, we introduce a data-driven approach inspired by RePaint [15], a diffusion-based image inpainting technique that effectively preserves background by explicitly incorporating forward-diffused background contexts in reverse diffusion process, instead of using them as conditional inputs [21]. We developed lesion-focused diffusion models, named LeFusion, specifically tailored for the synthesis of lesion textures. Unlike in RePaint, we have redesigned the diffusion learning objectives to be learnable solely from the lesion, reducing the learning complexity and improving the controllability. Given the interconnectedness given various lesion types, we further propose a strategy for the joint modeling of multi-class lesions through multi-channel decomposition. Moreover, we develop a generalized diffusion model for lesion masks capable of producing a diverse set. This enhancement increases the synthesis diversity and effectively improves the performance of downstream applications.

We validate our methodology using the cardiac lesion segmentation dataset provided by Emidec [14], which focuses on two specific lesion types in DE-MRI: myocardial infarction (MI) and persistent microvascular obstruction (PMO). Our results demonstrate that the pipeline we propose not only facilitates effective data augmentation of pathological scans but also enables synthetic pathology from normal ones. We use the popular nnUNet [10] to show that the resulting synthetic images make it possible to effectively boost a state-of-the-art model.

2 Method

2.1 Background: Controlled Lesion Synthesis (CLS)

Prior studies [33,9] aim to split lesion synthesis into separate texture and mask generation processes. This distinction facilitates lesion generation across both normal and pathological scans by relying on prior clinical knowledge, focusing on the creation of lesion masks and their textural content. Yet, these approaches

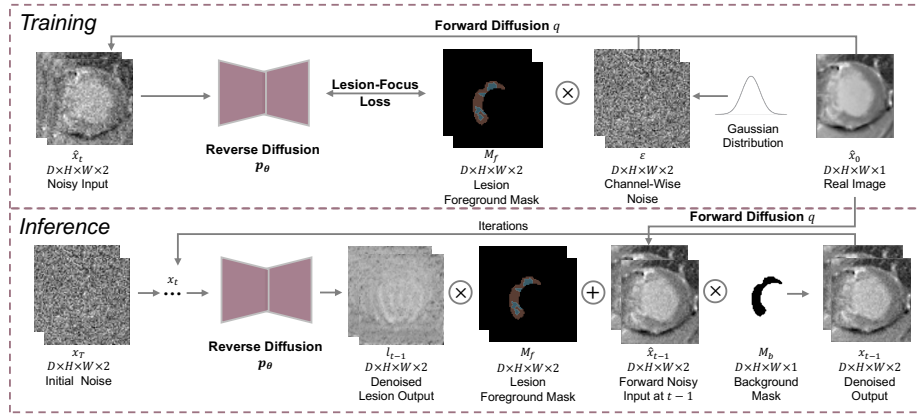


Fig. 1: **Illustration of Lesion-Focus Diffusion Model.** The top of the image illustrates the training process of the LeFusion, while the bottom depicts the inference process from the noise and the original image to the new image.

are predominantly manual. For texture synthesis, they [9] mainly depend on manually setting the texture’s grayscale values. Lesion shapes are crafted using morphological methods, involving the manual selection of ellipsoidal lesion masks and applying erosion and dilation techniques to soften the edges. This reliance on manual techniques restricts the advancement of controlled lesion synthesis.

2.2 LeFusion: Lesion-Focus Diffusion Model

Compared to previous handcrafted methods of controlled lesion synthesis [33,9], we have developed a framework that learns the texture and shape of lesions from data, enabling adaptation to various datasets. Our approach utilizes a repainting method which, theoretically, ensures that background information remains undisturbed, contrasting with earlier techniques. Additionally, we have designed a novel method for generating lesion masks that can automatically produce a diverse range of shapes closely resembling lesion masks. It is important to note that our proposed LeFusion supports the generation of multiple types of lesion masks and textures at the same time.

Disentangled Lesion and Background Generation. Inspired by diffusion-based inpainting [15], we aim to decouple the generation of lesion and background. As demonstrated in Fig. 1, inpainting aims to predict the missing parts of an image, particularly lesions, using a specified mask region as a condition. In this paper, we employ diffusion models [24] as a generative method. The inference process involves sampling a random noise vector $x_T \sim \mathcal{N}(0, 1)$ and gradually denoising it until achieving a high-quality output image x_0 . We refer to the original image with one channel as $\hat{x}_0 \in \mathbb{R}^{D \times H \times W \times 1}$, where D signifies the depth, H represents the height, and W denotes the width. For the diffusion model’s reverse step

from x_t to x_{t-1} , we decouple it into two components: lesion and background, as illustrated in the following equation. Here, M_f and M_b respectively represent the Lesion Foreground Mask and Background Mask. l_{t-1} is obtained from x_t through the reverse diffusion process p_θ utilizing a 3D U-Net, and \hat{x}_{t-1} is derived from \hat{x}_0 through the forward diffusion process q .

$$x_{t-1} = l_{t-1} \odot M_f + \hat{x}_{t-1} \odot M_b \quad (1)$$

Making Diffusion Model Lesion-Focus. However, the above method can not ensure the Denoised Output l_{t-1} focuses on the lesion area. Hence, we introduced a lesion focus loss into our model’s training process. The general training strategy for diffusion models starts with the original image \hat{x}_0 , continuously perturbing it by adding Gaussian noise with increasing variance over T time steps. Subsequently, a neural network is trained, conditioned on the noised version of the image at time step t , as well as the time step itself, to learn the noise distribution that perturbs the image, allowing the data distribution $p(x_{t-1}|x_t)$ at time $t-1$ to be inferred. During this training phase, the mask \hat{m}_1 is applied to ensure that the loss is calculated exclusively within the masked region. The training objective of our diffusion model is defined as follows, where $\epsilon \in \mathbb{R}^{D \times H \times W \times 1}$ signifies the channel-wise noise sourced from a Gaussian distribution.

$$\mathbb{E}_{\hat{x}_0, \epsilon \sim \mathcal{N}(0,1), t} \left[\|\hat{m}_1 \epsilon - \hat{m}_1 p_\theta(\hat{x}_t, t)\|_2^2 \right] \quad (2)$$

Joint Modeling of Multi-Class Lesions. The lesion-focused approach primarily targets the generation of single lesions. However, in many medical fields, there is a necessity to model multi-class lesions, such as MI and PMO in cardiac MRI studies. This approach does not capture the correlations between different lesions. To generate textures for multiple lesions simultaneously, we employ a joint modeling strategy for multi-class lesions, with each channel corresponding to a different lesion type. We expand the input image $\hat{x}_0 \in \mathbb{R}^{D \times H \times W \times 1}$ along the channel dimension based on the number of lesions (specifically 2 for this study) to obtain $\hat{x}_t \in \mathbb{R}^{D \times H \times W \times 2}$. The training objective of our diffusion model is defined as follows, where $n = 2$ represents the total number of lesions, and $\epsilon \in \mathbb{R}^{D \times H \times W \times 2}$ signifies the channel-wise noise sourced from a Gaussian distribution. Each \hat{m}_i is an element of M_f , with i varying from 1 to n .

$$\mathbb{E}_{\hat{x}_0, \epsilon \sim \mathcal{N}(0,1), t} \sum_{i=1}^n \left[\|\hat{m}_i \epsilon - \hat{m}_i p_\theta(\hat{x}_t, t)\|_2^2 \right] \quad (3)$$

2.3 Diffusion-Based Mask Synthesis

In this work, we introduce a novel framework for mask diffusion, named Diff-Mask. This innovative approach leverages the principles of diffusion models to specifically address the challenges of generating and refining masks in image and volume data. As shown in Fig. 2, we introduce the mask $M_m \in \mathbb{R}^{D \times H \times W \times 1}$ to constrain the generation of the lesion masks within the physiological structures

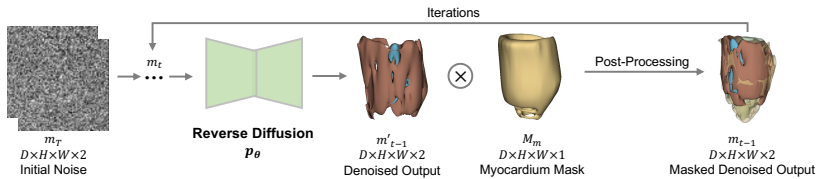


Fig. 2: Illustration of Diffusion-Based Lesion Mask Synthesis.

where lesions are likely to occur. Our approach employs multi-channel modeling to capture the shape correlations between multiple lesion masks and their spatial distribution and causal relationships (such as containment). Each channel is dedicated to generating a mask shape for a specific lesion, and we apply a smoothing kernel as a post-processing step to smooth the generated masks seamlessly. For the diffusion model’s reverse step from m_t to m_{t-1} , the training objective of our diffusion model is defined as follows, where n represents the number of lesion types and M_i belongs to M_m for $i = 1, 2$:

$$\mathbb{E}_{m_0, \epsilon \sim \mathcal{N}(0,1), t} \sum_{i=1}^n \left[\|M_i \epsilon - M_i p_\theta(m_t, t)\|_2^2 \right] \quad (4)$$

3 Experiments

3.1 Setup

Dataset. The Emidec dataset [14] consists of examinations featuring DE-MRI in a short-axis orientation. This dataset provides access to fully labeled data comprising a total of 100 cases, including 33 normal (**N**) and 67 pathological (**P**) cases. The annotations within the dataset cover five classes: background, left ventricle (LV), myocardium (Myo), myocardial infarction (MI), and persistent microvascular obstruction (PMO). We split the 67 pathological cases of the Emidec dataset into 57 for training and 10 for testing. The 57 pathological cases (P) are used to train the data synthesis model. In the downstream evaluation (Sec. 3.2), we use those models to synthesize pathological cases based on both 57 pathological (**P**) and 33 normal (**N**) as the downstream training set.

Method Comparison. The following image synthesis algorithms are compared with the proposed LeFusion-S/J.

Hand-Crafted [9]. The morphology of the lesion is represented by the overlapping of multiple ellipsoidal lesion masks, with the application of erosion and dilation techniques to blur the shapes. The texture is approximated using Gaussian noise and softened through interpolation and Gaussian filtering.

RePaint [15]. This approach removes the lesion mask from the image and then fills in the lesion texture through the process depicted in Fig. 1. The model employs global training loss, which lacks the capability to focus on lesion information. Due to the absence of guidance from lesion category information,

Table 1: **Downstream Cardiac Segmentation Dice (\uparrow) from DE-MRI on Emidec Dataset [14].** P: real pathological cases. P'/N': synthetic pathological cases from pathological/normal cases, using various synthetic approaches. N'': more synthetic data than N'. LeFusion-S/J: separate / joint modeling of multi-class lesions. The **bold** denote best performances on lesion region, and the **red** are those with significantly adverse effects compared to the baseline.

Methods	Training	Normal Region		Lesion Region	
		LV	Myo	MI	PMO
nnU-Net [10] Baseline	P	94.33	82.43	69.67	36.89
<i>Texture Synthesis with Real Masks on P'</i>					
Hand-Crafted [9]	P+P'	94.69	82.62	69.60	36.06
Cond-Diffusion [7,21]	P+P'	94.13	80.22	66.89	37.76
RePaint [15]	P+P'	94.72	82.55	69.14	28.93
LeFusion-S (Ours)	P+P'	94.59	82.20	69.88	34.79
LeFusion-J (Ours)	P+P'	94.63	82.38	69.95	38.01
<i>Texture Synthesis with Hand-Crafted Synthetic Masks [9] on N'</i>					
Hand-Crafted [9]	P+N'	94.31	80.77	68.19	35.73
Cond-Diffusion [7,21]	P+N'	94.08	79.69	67.41	31.03
LeFusion-S (Ours)	P+N'	94.45	81.82	69.17	37.18
LeFusion-J (Ours)	P+N'	94.66	82.40	69.87	37.31
<i>Enhanced with Diffusion-Based Synthetic Mask (DiffMask)</i>					
LeFusion-J+DiffMask (Ours)	P+N'	94.55	82.18	69.81	40.62
LeFusion-J+DiffMask (Ours)	P+N''	94.37	82.24	70.17	42.44
LeFusion-J+DiffMask (Ours)	P+P'+N''	94.43	82.24	70.34	43.54

it is unable to specify corresponding lesions and is confined to simulating the generation of single-class lesions

Cond-Diffusion [7,21]. Besides the method described above, which removes the lesion mask from the image and then fills in the texture, another approach involves using the lesion mask and background image information as conditional inputs [21] to a diffusion model [7]. Specifically, given a pair of an image x_0 and the mask of its lesion region m , the diffusion model is conditioned on both the mask m and the healthy region $x_{\text{health}} = (1 - m) \odot x_0$. The three features x_0 , m , and x_{health} are stacked together and fed into a 3D U-Net to infer the data distribution $p(x_{t-1}|x_t)$ at time $t - 1$ from t . The downside of this method is that it disrupts the background information. By directly using multiple masks as conditional inputs, it fails to control the corresponding categories and can only model the generation of single-class lesions.

LeFusion-S/J (Ours). For each lesion, individual models are trained separately for multiple texture generators, and then lesion texture information is filled in for each lesion location separately. The disadvantage is the lack of modeling for the correlation between textures across different lesions. Lesion-J is a generalized version to model multi-class lesions jointly.

Table 2: **Synthesis Image Quality Assessment from DE-MRI on Emidec Dataset [14]**. We compare the differences in image similarity between synthetic pathological cases generated by different methods given real pathological cases.

Methods	MI		PMO		Avg.	
	PSNR \uparrow	SSIM \uparrow	PSNR \uparrow	SSIM \uparrow	PSNR \uparrow	SSIM \uparrow
Hand-Crafted [9]	9.39	8.30	7.63	9.15	8.516	8.70
Cond-Diffusion [7,21]	13.25	46.92	8.00	9.23	10.62	28.07
RePaint [15]	19.81	80.68	15.23	70.27	17.52	75.47
LeFusion-S (Ours)	25.65	91.78	27.71	89.42	26.68	90.60
LeFusion-J (Ours)	28.30	91.41	35.23	93.23	31.77	92.32

3.2 Improving Cardiac Segmentation with Synthetic Data

We show that LeFusion is effective as augmenting training databases for the purpose of training nnUNet [10] to perform cardiac segmentation. We use the following synthetic subsets using various synthesis methods:

P': 57×1 synthetic cases from the 57 real pathological cases **P**; **N'**: 33×2 synthetic cases from the 33 normal cases **N**; **N''**: 33×5 synthetic cases from the 33 normal cases **N**.

We then use combinations of these subsets to train nnU-Net. The results are reported in Tab. 1 in terms of the Dice (0-100, higher is better).

In Tab. 1's first set, we apply texture synthesis with real masks. The Hand-Crafted [9] produces textures that differ from real textures, leading to a decrease in baseline performance. Cond-Diffusion [7,21] disrupts background structure, lowering Myo's Dice and blurring lesion categories, decreasing MI's performance. RePaint [15], focusing on global information, struggles to generate textures that conform to lesion characteristics, resulting in a significant decrease in the Dice for PMO lesions. LeFusion-S models the two lesions separately, ignoring the correlation between lesions, which leads to improved accuracy for MI but decreased accuracy for PMO lesions. In contrast, our proposed LeFusion-J achieves superior results; For the second group, we expanded the normal data utilizing texture synthesis with hand-crafted synthetic masks. Due to RePaint [15]'s inability to distinguish between multiple lesion categories, we did not repeat experiments for it. From the experiments, we observed results similar to those of the first group; For the last, we evaluated our proposed lesion mask synthesis. Our method significantly improved the performance for both MI and PMO. Additionally, as data volume expanded, downstream segmentation Dice consistently improved.

3.3 Synthesis Quality Assessment

Image Quality. As shown in Tab. 2, we selected Peak Signal-to-Noise Ratio (PSNR) and Structural Similarity Index Measure (SSIM) to calculate the similarity between synthetic pathological cases generated by different methods and real pathological cases. Our proposed LeFusion-J achieved the highest average

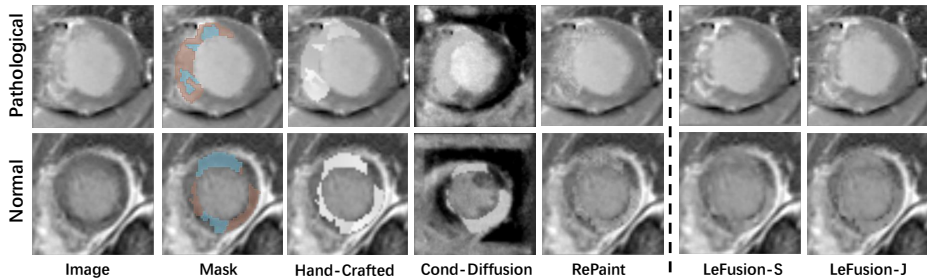


Fig. 3: **Visualization of Synthetic Images Given Lesion Masks.** Masks are real one on the pathological, and synthetic on the normal. Our LeFusion are compared with Hand-Crafted [9], Cond-Diffusion [7,21] and RePaint [15].

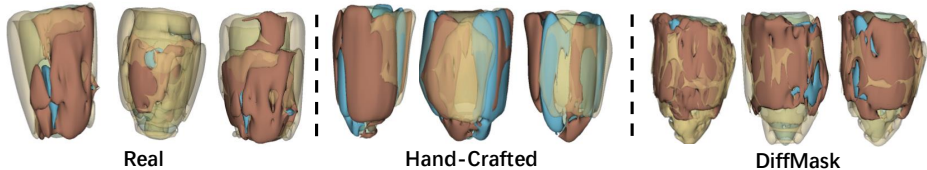


Fig. 4: **Visualization of Real / Synthetic Lesion Masks.** From left to right, the images respectively show the real pathological mask, hand-crafted [9] synthesized mask, and our diffusion-generated mask.

PSNR and SSIM. Fig. 3 displays the synthesized visualization of two lesions: MI (blue) and PMO (red). The Cond-Diffusion method [7,21] disrupts the background structure. The lesions generated by Hand-Crafted [9] and RePaint [15] fail to capture texture information, such as the grayscale variations characteristic of the lesions. In contrast, LeFusion-J more accurately reflects the textures of both lesion types and, compared to LeFusion-S, results in smoother transitions at the boundaries between the two lesions and with the background. More visualizations can be found in the supplementary materials.

Mask Quality. We also visualize synthetic lesion masks, as shown in Fig. 4. Compared to the hand-crafted masks [9], our diffusion-generated masks are closer to the real masks and exhibit a more diverse range of shape patterns.

4 Discussion & Conclusion

Concurrent Work. A recent study [2] employs conditional diffusion [7,21] to synthesize abdomen tumors, building on the controlled lesion synthesis framework [33,9]. In their approach, the diffusion process is not lesion-focus, learning both the background and the lesion, with the lesion mask and the background image (minus the lesion part) serving as conditional inputs. The preservation of

background can not be theoretically guaranteed. Despite differences in applications and implementation details, *e.g.* the use of encoded latent diffusion [21], this approach is essentially Cond-Diffusion as described. From our findings, it struggles to ensure high-quality background generation (Fig. 3), and may potentially lead to adverse effects in downstream applications (Tab. 1).

Conclusion. In conclusion, we introduce LeFusion, a novel lesion-focused diffusion models capable by recalibrating the diffusion learning objectives to target lesion areas. It preserves background by integrating forward-diffused background contexts into the reverse diffusion process. Our methodology is extended to handle multi-class lesions jointly, and further enhanced by a generative model for lesion masks, significantly broadening the diversity of our synthetic data. We demonstrate that synthetic data generated by our method can effectively boost the performance of a state-of-the-art network like nnU-Net.

Acknowledgment. This research was supported in part by a Swiss National Science Foundation grant.

References

1. Billot, B., Greve, D.N., Puonti, O., Thielscher, A., Van Leemput, K., Fischl, B., Dalca, A.V., Iglesias, J.E., et al.: Synthseg: Segmentation of brain mri scans of any contrast and resolution without retraining. *Medical Image Analysis* **86**, 102789 (2023)
2. Chen, Q., Chen, X., Song, H., Xiong, Z., Yuille, A., Wei, C., Zhou, Z.: Towards generalizable tumor synthesis. arXiv preprint arXiv:2402.19470 (2024)
3. Chen, R.J., Wang, J.J., Williamson, D.F., Chen, T.Y., Lipkova, J., Lu, M.Y., Sahai, S., Mahmood, F.: Algorithmic fairness in artificial intelligence for medicine and healthcare. *Nature biomedical engineering* **7**(6), 719–742 (2023)
4. Du, Y., Jiang, Y., Tan, S., Wu, X., Dou, Q., Li, Z., Li, G., Wan, X.: Arsdm: colonoscopy images synthesis with adaptive refinement semantic diffusion models. In: *International conference on medical image computing and computer-assisted intervention*. pp. 339–349. Springer (2023)
5. Goodfellow, I., Pouget-Abadie, J., Mirza, M., Xu, B., Warde-Farley, D., Ozair, S., Courville, A., Bengio, Y.: Generative adversarial networks. *Communications of the ACM* **63**(11), 139–144 (2020)
6. Han, C., Kitamura, Y., Kudo, A., Ichinose, A., Rundo, L., Furukawa, Y., Umemoto, K., Li, Y., Nakayama, H.: Synthesizing diverse lung nodules wherever massively: 3d multi-conditional gan-based ct image augmentation for object detection. In: *International Conference on 3D Vision*. pp. 729–737. IEEE (2019)
7. Ho, J., Jain, A., Abbeel, P.: Denoising diffusion probabilistic models. *Advances in Neural Information Processing Systems* **33**, 6840–6851 (2020)
8. Horvath, I., Paetzold, J., Schoppe, O., Al-Maskari, R., Ezhov, I., Shit, S., Li, H., Ertürk, A., Menze, B.: Metgan: generative tumour inpainting and modality synthesis in light sheet microscopy. In: *IEEE Winter Conference on Applications of Computer Vision*. pp. 227–237 (2022)
9. Hu, Q., Chen, Y., Xiao, J., Sun, S., Chen, J., Yuille, A.L., Zhou, Z.: Label-free liver tumor segmentation. In: *Conference on Computer Vision and Pattern Recognition*. pp. 7422–7432 (2023)

10. Isensee, F., Jaeger, P.F., Kohl, S.A., Petersen, J., Maier-Hein, K.H.: nnu-net: a self-configuring method for deep learning-based biomedical image segmentation. *Nature methods* **18**(2), 203–211 (2021)
11. Jin, Q., Cui, H., Sun, C., Meng, Z., Su, R.: Free-form tumor synthesis in computed tomography images via richer generative adversarial network. *Knowledge-Based Systems* **218**, 106753 (2021)
12. Khader, F., Müller-Franzes, G., Tayebi Arasteh, S., Han, T., Haarbuerger, C., Schulze-Hagen, M., Schad, P., Engelhardt, S., Baeßler, B., Foersch, S., et al.: Denoising diffusion probabilistic models for 3d medical image generation. *Scientific Reports* **13**(1), 7303 (2023)
13. Kingma, D.P., Welling, M.: Auto-encoding variational bayes. *arXiv Preprint* (2013)
14. Lalande, A., Chen, Z., Pommier, T., Decourselle, T., Qayyum, A., Salomon, M., Ginjac, D., Skandarani, Y., Boucher, A., Brahim, K., et al.: Deep learning methods for automatic evaluation of delayed enhancement-mri. the results of the emidec challenge. *Medical Image Analysis* **79**, 102428 (2022)
15. Lugmayr, A., Danelljan, M., Romero, A., Yu, F., Timofte, R., Van Gool, L.: Repaint: Inpainting using denoising diffusion probabilistic models. In: *Conference on Computer Vision and Pattern Recognition*. pp. 11461–11471 (2022)
16. Lyu, F., Ye, M., Carlsen, J.F., Erleben, K., Darkner, S., Yuen, P.C.: Pseudo-label guided image synthesis for semi-supervised covid-19 pneumonia infection segmentation. *IEEE Transactions on Medical Imaging* **42**(3), 797–809 (2022)
17. Lyu, F., Ye, M., Ma, A.J., Yip, T.C.F., Wong, G.L.H., Yuen, P.C.: Learning from synthetic ct images via test-time training for liver tumor segmentation. *IEEE Transactions on Medical Imaging* **41**(9), 2510–2520 (2022)
18. Pishva, A.K., Thambawita, V., Torresen, J., Hicks, S.A.: Repolyp: A framework for generating realistic colon polyps with corresponding segmentation masks using diffusion models. In: *2023 IEEE 36th International Symposium on Computer-Based Medical Systems (CBMS)*. pp. 47–52. IEEE (2023)
19. Price, W.N., Cohen, I.G.: Privacy in the age of medical big data. *Nature medicine* **25**(1), 37–43 (2019)
20. Qayyum, A., Qadir, J., Bilal, M., Al-Fuqaha, A.: Secure and robust machine learning for healthcare: A survey. *IEEE Reviews in Biomedical Engineering* **14**, 156–180 (2020)
21. Rombach, R., Blattmann, A., Lorenz, D., Esser, P., Ommer, B.: High-resolution image synthesis with latent diffusion models. In: *Conference on Computer Vision and Pattern Recognition*. pp. 10684–10695 (2022)
22. Savage, N.: Synthetic data could be better than real data. *Nature* (2023), <https://doi.org/10.1038/d41586-023-01445-8>
23. Shin, Y., Qadir, H.A., Balasingham, I.: Abnormal colon polyp image synthesis using conditional adversarial networks for improved detection performance. *IEEE Access* **6**, 56007–56017 (2018)
24. Sohl-Dickstein, J., Weiss, E., Maheswaranathan, N., Ganguli, S.: Deep unsupervised learning using nonequilibrium thermodynamics. In: *International conference on machine learning*. pp. 2256–2265. PMLR (2015)
25. Suriyakumar, V.M., Papernot, N., Goldenberg, A., Ghassemi, M.: Chasing your long tails: Differentially private prediction in health care settings. In: *Proceedings of the 2021 ACM Conference on Fairness, Accountability, and Transparency*. pp. 723–734 (2021)
26. Wang, H., Zhou, Y., Zhang, J., Lei, J., Sun, D., Xu, F., Xu, X.: Anomaly segmentation in retinal images with poisson-blending data augmentation. *Medical Image Analysis* **81**, 102534 (2022)

27. Weng, Z., Yang, J., Liu, D., Cai, W.: Topology repairing of disconnected pulmonary airways and vessels: Baselines and a dataset. In: Conference on Medical Image Computing and Computer Assisted Intervention. pp. 382–392. Springer (2023)
28. Xu, J., Xiao, Y., Wang, W.H., Ning, Y., Shenkman, E.A., Bian, J., Wang, F.: Algorithmic fairness in computational medicine. *EBioMedicine* **84** (2022)
29. Yang, J., Shi, R., Ni, B.: Medmnist classification decathlon: A lightweight auttml benchmark for medical image analysis. In: International Symposium on Biomedical Imaging. pp. 191–195. IEEE (2021)
30. Yang, J., Shi, R., Wei, D., Liu, Z., Zhao, L., Ke, B., Pfister, H., Ni, B.: Medmnist v2- a large-scale lightweight benchmark for 2d and 3d biomedical image classification. *Scientific Data* **10**(1), 41 (2023)
31. Yang, J., Liu, S., Grbic, S., Setio, A.A.A., Xu, Z., Gibson, E., Chabin, G., Georgescu, B., Laine, A.F., Comaniciu, D.: Class-aware adversarial lung nodule synthesis in ct images. In: International Symposium on Biomedical Imaging. pp. 1348–1352. IEEE (2019)
32. Yang, Z., Pan, J., Yang, Y., Shi, X., Zhou, H.Y., Zhang, Z., Bian, C.: Proco: Prototype-aware contrastive learning for long-tailed medical image classification. In: International Conference on Medical Image Computing and Computer-Assisted Intervention. pp. 173–182. Springer (2022)
33. Yao, Q., Xiao, L., Liu, P., Zhou, S.K.: Label-free segmentation of covid-19 lesions in lung ct. *IEEE Transactions on Medical Imaging* **40**(10), 2808–2819 (2021)
34. Zhang, Y., Kang, B., Hooi, B., Yan, S., Feng, J.: Deep long-tailed learning: A survey. *IEEE Transactions on Pattern Analysis and Machine Intelligence* (2023)

Appendix

LeFusion: Synthesizing Myocardial Pathology on Cardiac MRI via Lesion-Focus Diffusion Models

Hantao Zhang, Jiancheng Yang, Shouhong Wan, and Pascal Fua

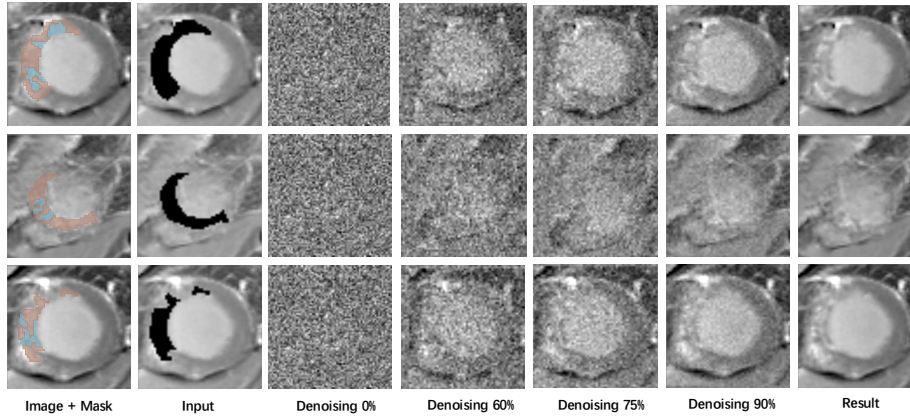


Fig. A1: **Visualization of the Denoising Process in LeFusion for Inpainting.** The process is conditioned on the masked input. Starting from a random Gaussian noise sample, the procedure iteratively denoises this input, progressively refining it into a high-quality image with the lesions.

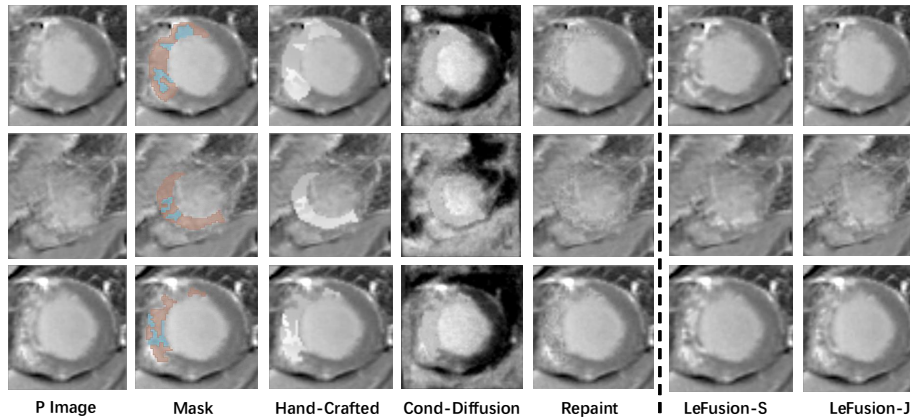


Fig. A2: **Visualization of Synthetic Images Given Real Lesion Masks on Pathological Cases.** Our LeFusion are compared with Hand-Crafted [9], Cond-Diffusion [7,21] and RePaint [15].

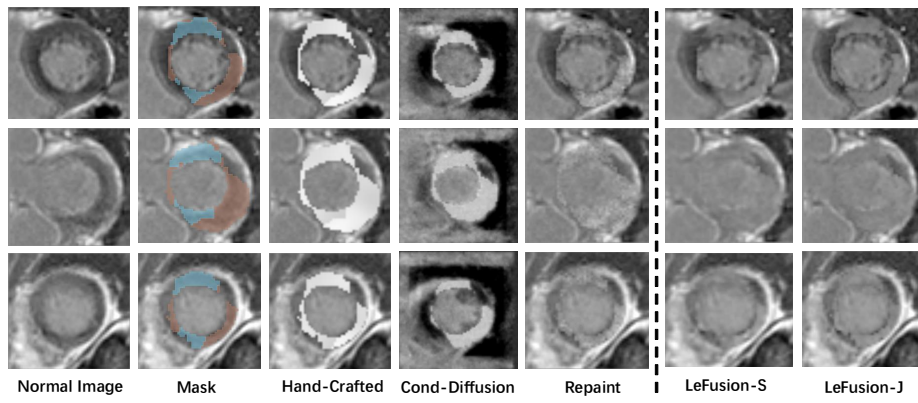


Fig. A3: **Visualization of Synthetic Images Given Synthetic Lesion Masks on Normal Cases.** Our LeFusion are compared with Hand-Crafted [9], Cond-Diffusion [7,21] and RePaint [15].